

Density Functional Theory Study of the Mechanisms and Stereochemistry of the Rh(I)-Catalyzed Intramolecular [3+2] Cycloadditions of 1-Ene- and 1-Yne-Vinylcyclopropanes

Lei Jiao, Mu Lin, and Zhi-Xiang Yu*

Beijing National Laboratory for Molecular Sciences (BNLMS), Key Laboratory of Bioorganic Chemistry and Molecular Engineering of Ministry of Education, College of Chemistry, Peking University, Beijing 100871, China

Received August 25, 2010; E-mail: yuzx@pku.edu.cn

Abstract: The mechanisms, structures of all stationary points involved, and kinetic and thermodynamic parameters of the Rh(I)-catalyzed intramolecular [3+2] cycloaddition reactions of 1-ene- and 1-yne-vinylcyclopropanes (1-ene-VCPs and 1-yne-VCPs) have been investigated using density functional theory (DFT) calculations. The computational results showed that the [3+2] reactions of 1-ene/yne-VCPs studied here occur through a catalytic cycle of substrate–catalyst complex formation, cyclopropane cleavage, alkene/alkyne insertion, and reductive elimination. Alkene/alkyne insertion is the rate- and stereoselectivity-determining step of these multistep [3+2] cycloadditions. The experimentally observed high reactivity of 1-yne-VCPs compared to 1-ene-VCPs is well rationalized by the differences of steric effects in the alkyne/alkene insertion transition states. DFT calculations unveiled that the relative orientation of the tethers in the 1-ene/yne-VCPs plays a key role in controlling the stereochemistry of the [3+2] cycloadducts. In addition, DFT calculation results are used to explain why, in some cases, the formation of the β -hydride elimination byproduct can compete with the [3+2] pathway.

Introduction

Transition-metal-catalyzed cycloaddition reactions constitute an important part of modern organic synthesis. In particular, using small-ring compounds as cycloaddition partners brings opportunities for developing novel reactions that complement or surpass traditional cycloadditions.^{1,2} Among them, the combination of Rh(I) catalysis and vinylcyclopropane (VCP) provides a variety of efficient methods for constructing six- to eight-membered-ring structures (Figure 1). For instance, VCP derivatives have been found to undergo a wide array of intra- and intermolecular [5+1],³ [5+2],⁴ [5+2+1],⁵ and [5+1+2+1]⁶ cycloaddition reactions under Rh(I) catalysis, where the VCP moiety usually acts as a five-carbon component (Figure 1).

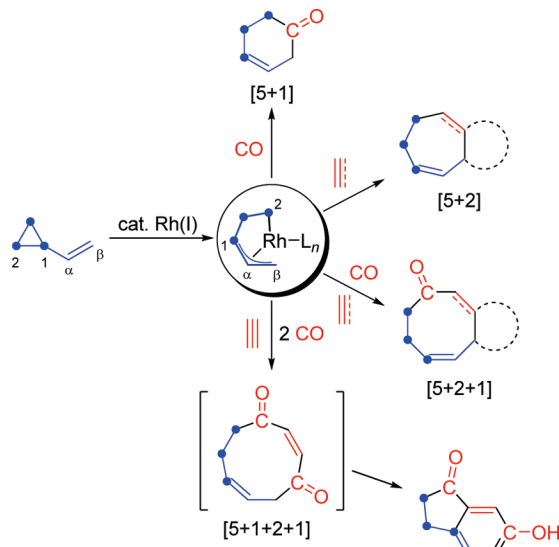
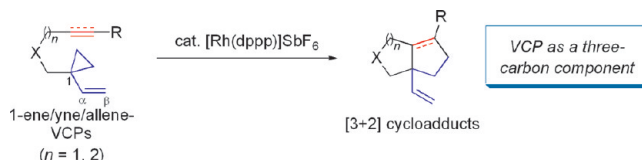


Figure 1. Rh(I)-catalyzed cycloadditions employing VCP as a five-carbon unit.

- (1) (a) Lautens, M.; Klute, W.; Tam, W. *Chem. Rev.* **1996**, *96*, 49. (b) *Small Ring Compounds in Organic Synthesis V*; Topics in Current Chemistry 178; de Meijere, A., Ed.; Springer-Verlag: Berlin, 1996. (c) *Small Ring Compounds in Organic Synthesis VI*; Topics in Current Chemistry 207; de Meijere, A., Ed.; Springer-Verlag: Berlin, 2000. (d) Reissig, H.-U.; Zimmer, R. *Chem. Rev.* **2003**, *103*, 1151. (e) Rubin, M.; Rubina, M.; Gevorgyan, V. *Chem. Rev.* **2007**, *107*, 3117. (f) Yu, Z.-X.; Wang, Y.; Wang, Y. *Chem. Asian J.* **2010**, *5*, 1072.
- (2) Here we refer to the transition-metal-catalyzed cycloaddition reactions as the [m+n] cycloaddition, where brackets, instead of parentheses, are used in the nomenclature. Although m and n do not stand for the number of electrons involved in these cycloadditions, we prefer to follow the traditional nomenclature of the most original publications, where brackets were used.
- (3) (a) Ben-Shoshan, R.; Sarel, S. *J. Chem. Soc., Chem. Commun.* **1969**, 883. (b) Victor, R.; Ben-Shoshan, R.; Sarel, S. *Tetrahedron Lett.* **1970**, *11*, 4253. (c) Sarel, S. *Acc. Chem. Res.* **1978**, *11*, 204. (d) Aumann, R. *J. Am. Chem. Soc.* **1974**, *96*, 2631. (e) Taber, D. F.; Kanai, K.; Jiang, Q.; Bui, G. *J. Am. Chem. Soc.* **2000**, *122*, 6807. (f) Taber, D. F.; Joshi, P. V.; Kanai, K. *J. Org. Chem.* **2004**, *69*, 2268. (g) Kurahashi, T.; de Meijere, A. *Synlett* **2005**, 2619.

These reactions have great synthetic potential in organic synthesis, as evidenced by their applications in a number of natural product syntheses as the key skeleton-building steps.⁷ Through investigating the [5+2] reaction mechanisms with the aid of DFT calculations,⁸ Houk and Wender found that these [5+2] reactions usually involve Rh(I)-catalyzed cyclopropane ring-opening to give six-membered rhodacycles (Figure 1, intermediate in the circle), which can then be intercepted by various cycloaddition components. Through further elementary

Scheme 1. Rh(I)-Catalyzed Intramolecular [3+2] Cycloaddition Reactions of 1-Ene/Yne/Allene-VCPs



steps (such as insertion and reductive elimination), six- to nine-membered cyclic compounds can be finally obtained.

Recently, we discovered that a new type of VCP derivative, 1-ene/yne/allene-VCPs, can undergo a novel intramolecular [3+2] cycloaddition reaction to furnish cyclopentane- or cyclopentene-embedded 5,5- and 6,5-bicyclic structures (Scheme 1).⁹ In these [3+2] reactions, the VCP moiety serves as a three-carbon unit,¹⁰ rather than the traditional five-carbon unit. These reactions provide very efficient methods for the construction of multisubstituted five-membered rings, especially those with a quaternary bridgehead carbon center.

In this paper, we report our DFT studies of the mechanisms and stereochemistry of these [3+2] reactions shown in Scheme 1. Our first aim in this mechanistic study was to fully understand the mechanisms of the [3+2] cycloadditions at the molecular level. The catalytic cycles of 1-ene/yne-VCP cycloadditions were proposed previously by invoking the generally accepted mechanism of the Rh(I)/vinylcyclopropane chemistry (Figure 2).⁸ We proposed that the [3+2] reaction of 1-ene/yne-VCPs commences with a ligand exchange reaction between the product–Rh(I) complex **IN4** and the substrate. Through this process, the final [3+2] cycloadduct is released, and the starting substrate–Rh(I) complex **IN1** is generated. Cyclopropane cleavage then takes place, giving a π -allyl–Rh(I) complex **IN2**, which is then transformed to **IN3** through insertion of olefin/alkyne into the Rh–C1 bond in **IN2**. Finally, reductive elimination generates a C(sp³)–C(sp³) or C(sp²)–C(sp³) bond to afford the product–Rh(I) complex **IN4**. A new catalytic cycle will then start from the exchange reaction between **IN4** and 1-ene/yne-VCP substrate. We provide full details of these

Table 1. Previous Optimization of the Reaction Conditions for the [3+2] Cycloaddition of 1-Ene-VCP^a

entry	catalyst	t (°C)	time (h)	ratio 2:3 ^b	yield (%) ^c
1	[Rh(CO) ₂ Cl] ₂	110 ^d	4.5	4:1	57
2	[Rh(CO) ₂]SbF ₆	80	1	1:1	15
3	[Rh(NBD)]SbF ₆	80	2	5:1	38
4	[Rh(dppp)]SbF ₆	80	2	40:1	93

^a Reaction conditions: 5 mol % Rh(I) catalyst, anhydrous dichloroethane (DCE) as solvent (substrate concentration 0.05 M), argon atmosphere. ^b Determined by ¹H NMR. ^c Combined isolated yield of inseparable product mixture of **2** and **3**. ^d Toluene as solvent.

multistep reactions obtained from DFT calculations, including the potential energy surfaces, the geometric information of the intermediates and transition structures, and the rate- and stereoselectivity-determining steps. In addition, in these reactions, the unusual cycloaddition selectivity of the VCP moiety serving as a three-carbon synthon, instead of a five-carbon synthon, will be elucidated through the DFT calculations.

Furthermore, we used the computed mechanistic insights to rationalize the intriguing but very puzzling experimental observations reported in our previous communication. During catalyst screening using 1-ene-VCP **1** as the substrate, we found that [Rh(dppp)]SbF₆ (dppp = 1,3-bis(diphenylphosphino)propane) is the optimal catalyst for the intramolecular [3+2] cycloadditions. Other neutral and cationic Rh(I) species are less efficient for the target reaction, and a remarkable amount of β -hydride elimination byproduct **3** is generated using these as catalysts (Table 1, entries 1–3). We assume that this side product is generated through the β -hydride elimination pathway from intermediate **IN3** (Figure 2). In this competitive pathway, **IN3** first undergoes a β -hydride elimination to give **IN5**, which then gives rise to the diene product **3** via a reductive elimination process. However, the reason why different Rh complexes have

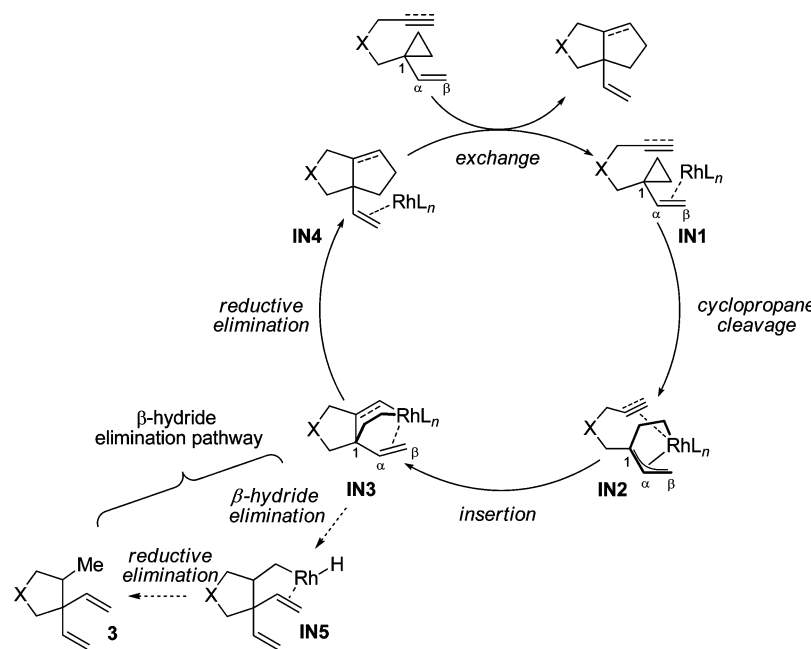
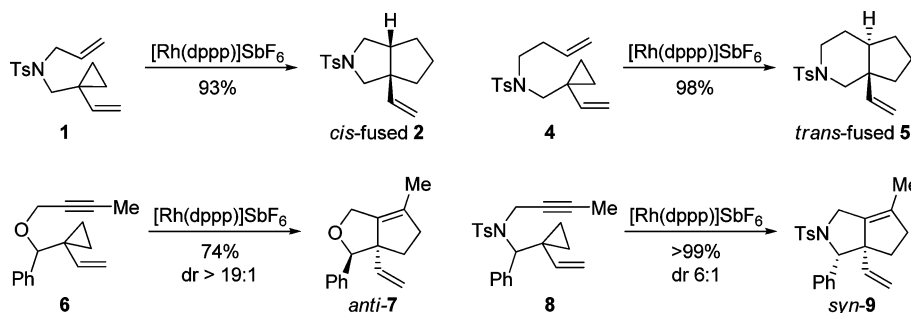


Figure 2. [3+2] catalytic cycles employing 1-ene/yne-VCPs as the substrates.

Scheme 2. Previously Observed Stereochemistry of the Rh(I)-Catalyzed [3+2] Intramolecular Cycloadditions

different reaction profiles was unknown. Therefore, detailed DFT calculations of this β -hydride elimination pathway are required to demystify these experimental puzzles.

Another intriguing experimental finding is related to the diverse substrate-dependent diastereoselectivities in the [3+2] cycloadditions (Scheme 2). When 1-ene-VCPs are employed as substrates, formation of a 5,5-bicyclic system favors cis ring-fused cycloadduct (**1**→**2**), while formation of a 6,5-bicyclic system favors trans ring-fused cycloadduct (**4**→**5**). When 1-yne-VCPs are employed as substrates, interestingly, the stereoinduction by a preexisting chiral center neighboring to the C(1) atom is determined by the tether group in 1-yne-VCP: oxygen-tethered 1-yne-VCP **6** gives anti diastereoselection (**6**→**7**), while tosylamide-tethered 1-yne-VCP **8** affords syn diastereoselection (**8**→**9**). The key factors influencing the diastereoselectivity of these [3+2] cycloadditions are not known, and thus a detailed computational investigation is required.

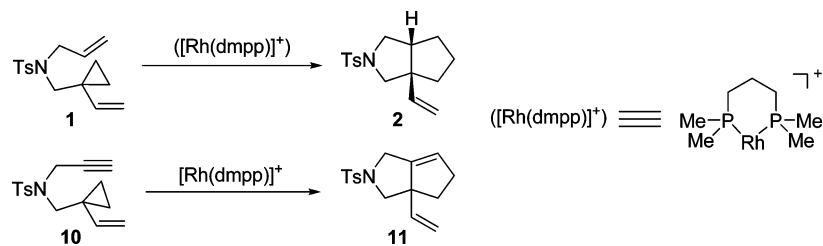
Therefore, we conducted DFT mechanistic investigations of the Rh(I)-catalyzed intramolecular [3+2] cycloadditions of 1-ene/yne-VCP substrates and report herein the results of our computational study. The results presented here not only provide insightful mechanistic information to rationalize the experimental observations of these intriguing reactions but also give guidance and inspiration for design and development of new reactions. In addition, we believe that this study will help the future development of asymmetric [3+2] cycloaddition reactions using chiral bidentate phosphine ligands.

Computational Details

All calculations were performed with the Gaussian 03 program.¹¹ Density functional theory calculations using the B3LYP functional¹²

were used to locate all the stationary points involved. The 6-31G(d) basis set was applied for all elements except for Rh, for which the LANL2DZ¹³ basis set was used. This approach has been successfully applied to study structures and reaction mechanisms for reactions of carbonyl rhodium(I) complexes and other Rh-catalyzed cycloadditions.^{8,14} Frequency calculations at the same level were performed to confirm each stationary point to be either a minimum or a transition structure. Solvation energies in 1,2-dichloroethane were evaluated by a self-consistent reaction field (SCRF) using the CPCM model,¹⁵ where the simple united atom topological model (UA0) was used to define the atomic radii. Solvation calculations were carried out on the gas-phase optimized structures. The reported energies are the zero-point energy-corrected enthalpies (ΔH_{gas}),

- (7) For representative natural product synthesis using the Rh(I)-catalyzed [5+2] cycloadditions of vinylcyclopropane derivatives, see: (a) Wender, P. A.; Fuji, M.; Husfeld, C. O.; Love, J. A. *Org. Lett.* **1999**, *1*, 137. (b) Wender, P. A.; Zhang, L. *Org. Lett.* **2000**, *2*, 2323. (c) Ashfeld, B. L.; Martin, S. F. *Org. Lett.* **2005**, *7*, 4535. (d) Trost, B. M.; Waser, J.; Meyer, A. *J. Am. Chem. Soc.* **2007**, *129*, 14556. (e) Trost, B. M.; Waser, J.; Meyer, A. *J. Am. Chem. Soc.* **2008**, *130*, 16424. For natural product synthesis using the Rh(I)-catalyzed [(5+2)+1] cycloaddition, see: (f) Jiao, L.; Yuan, C.; Yu, Z.-X. *J. Am. Chem. Soc.* **2008**, *130*, 4421. (g) Fan, X.; Tang, M.-X.; Zhuo, L.-G.; Tu, Y. Q.; Yu, Z.-X. *Tetrahedron Lett.* **2009**, *50*, 155. (h) Fan, X.; Zhuo, L.-G.; Tu, Y. Q.; Yu, Z.-X. *Tetrahedron* **2009**, *65*, 4709. (i) Yuan, C.; Jiao, L.; Yu, Z.-X. *Tetrahedron Lett.* **2010**, *51*, 5674.
- (8) (a) Yu, Z.-X.; Wender, P. A.; Houk, K. N. *J. Am. Chem. Soc.* **2004**, *126*, 9154. (b) Yu, Z.-X.; Cheong, P. H.-Y.; Liu, P.; Legault, C. Y.; Wender, P. A.; Houk, K. N. *J. Am. Chem. Soc.* **2008**, *130*, 2378. (c) Liu, P.; Cheong, P. H.-Y.; Yu, Z.-X.; Wender, P. A.; Houk, K. N. *Angew. Chem., Int. Ed.* **2008**, *47*, 3939. (d) Liu, P.; Sirois, L. E.; Cheong, P. H.-Y.; Yu, Z.-X.; Hartung, I. V.; Rieck, H.; Wender, P. A.; Houk, K. N. *J. Am. Chem. Soc.* **2010**, *132*, 10127.
- (9) Jiao, L.; Lin, M.; Yu, Z.-X. *Chem. Commun.* **2010**, *46*, 1059.
- (10) For other reactions of VCPs acting as three-carbon synthons, see: (a) Jiao, L.; Ye, S.; Yu, Z.-X. *J. Am. Chem. Soc.* **2008**, *130*, 7178. (b) Li, Q.; Jiang, G.-J.; Jiao, L.; Yu, Z.-X. *Org. Lett.* **2010**, *12*, 1332. (c) Jiao, L.; Lin, M.; Zhuo, L.-G.; Yu, Z.-X. *Org. Lett.* **2010**, *12*, 2528.
- (11) Frisch, M. J.; et al. *Gaussian 03*, Revision C.02; Gaussian Inc.: Wallingford, CT, 2004.
- (12) (a) Becke, A. D. *J. Chem. Phys.* **1993**, *98*, 5648. (b) Lee, C.; Yang, W.; Parr, R. G. *Phys. Rev. B* **1988**, *37*, 785.
- (13) (a) Hay, P. J.; Wadt, W. R. *J. Chem. Phys.* **1985**, *82*, 299. (b) Dunning, T. H., Jr.; Hay, P. J. In *Modern Theoretical Chemistry*; Schaefer, H. F., III, Ed.; Plenum Press: New York, 1977; pp 1–28.
- (14) (a) Nakamura, E.; Yoshikai, N.; Yamanaka, M. *J. Am. Chem. Soc.* **2002**, *124*, 7181. (b) Baik, M.-H.; Baum, E. W.; Burland, M. C.; Evans, P. A. *J. Am. Chem. Soc.* **2005**, *127*, 1602. (c) Montero-Campillo, M. M.; Rodriguez-Otero, J.; Cabaleiro-Lago, E. M. *Tetrahedron* **2008**, *64*, 6215. (d) Wang, H.; Sawyer, J. R.; Evans, P. A.; Baik, M.-H. *Angew. Chem., Int. Ed.* **2008**, *47*, 342. (e) Montero-Campillo, M. M.; Cabaleiro-Lago, E. M.; Rodriguez-Otero, J. *J. Phys. Chem. A* **2008**, *112*, 9068. (f) Liang, Y.; Zhou, H.; Yu, Z.-X. *J. Am. Chem. Soc.* **2009**, *131*, 17783. (g) Hansen, J.; Autschbach, J.; Davies, H. M. L. *J. Org. Chem.* **2009**, *74*, 6555.
- (15) (a) Barone, V.; Cossi, M. *J. Phys. Chem. A* **1998**, *102*, 1995. (b) Cossi, M.; Rega, N.; Scalmani, G.; Barone, V. *J. Comput. Chem.* **2003**, *24*, 669. (c) Takano, Y.; Houk, K. N. *J. Chem. Theory Comput.* **2005**, *1*, 70.
- (16) See Supporting Information for a detailed discussion on the active catalytic species.

Scheme 3. Model Reactions Investigated in Our DFT Study

Gibbs free energies ($\Delta G_{\text{gas} \ 298\text{K}}$), both in the gas phase, and the Gibbs free energies in 1,2-dichloroethane solution ($\Delta G_{\text{sol} \ 298\text{K}}$). Unless specifically mentioned, all discussed relative energies in this paper are referred to $\Delta G_{\text{sol} \ 298\text{K}}$.

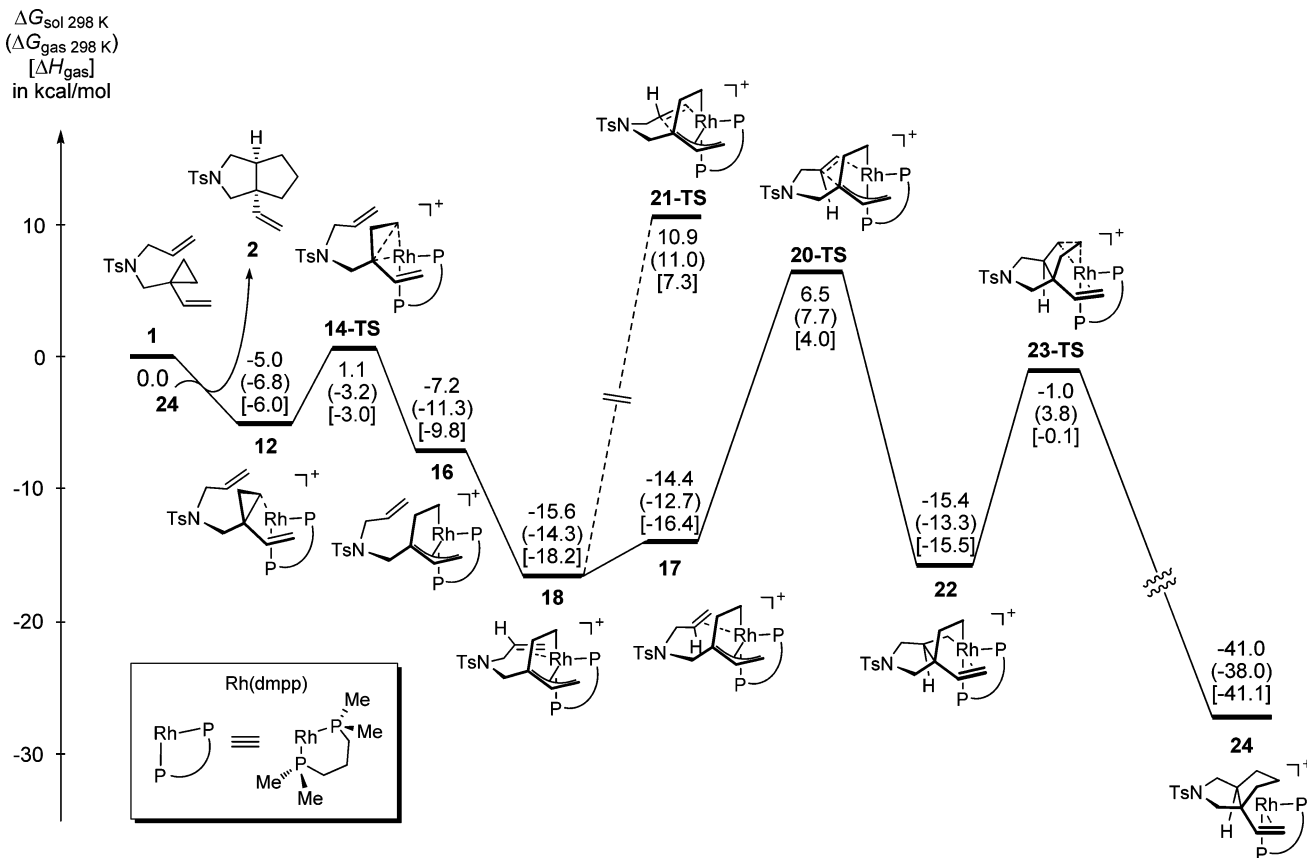
Results and Discussion

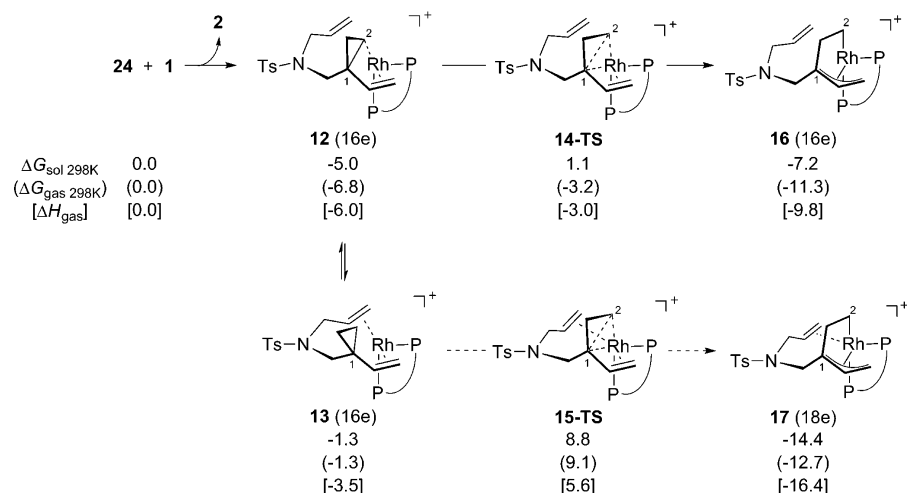
In previous experiments, the catalyst for the [3+2] reactions was prepared by the reaction of $[\text{Rh}(\text{CO})_2\text{Cl}]_2$ and AgSbF_6 in the presence of the bidentate phosphine ligand, dppp. We believe that the catalytic species involved in the reaction is a cationic species, $[\text{Rh}(\text{dppp})]^+$, which is generated by dissociation of CO from the rhodium center.¹⁶

Two model [3+2] reactions of 1-ene-VCP **1** and 1-yne-VCP **10** (Scheme 3) have been investigated using DFT calculations to address issues mentioned in the Introduction. Experimentally, the catalyst for all reported [3+2] reactions is $[\text{Rh}(\text{dppp})]\text{SbF}_6$. To save computational time but without sacrificing credibility of the present DFT investigation, the four phenyl groups in the dppp ligand are replaced by methyl groups. Therefore, the model catalyst for our investigation is $[\text{Rh}(\text{dmpp})]^+$, which is also

shown in Scheme 3. The counterion of the catalyst, SbF_6^- , is believed to act as a spectator and thus is not considered in the calculations.

In the following sections, we will first discuss the DFT-computed energy surfaces of the intramolecular [3+2] cycloaddition reaction of 1-ene-VCP (Part 1), aiming to elucidate the details of each elementary step, the structures of stationary points, the rate- and stereodetermining step, and thermodynamics and kinetics of this reaction (section 1.1). The origin of ring-fusion stereoselectivity in the formation of 5,5- and 5,6-bicyclic systems will then be presented and analyzed (section 1.2). Also in this part, DFT study of the β -hydride elimination pathway, which is a side reaction of the [3+2] reaction, will be discussed to disclose how this pathway competes with the [3+2] pathway and how different ligands affect this competition (section 1.3). In Part 2, we will present the full potential energy surface of the [3+2] cycloaddition of 1-yne-VCP. Through comparing the potential energy surfaces of the [3+2] reactions of 1-ene-VCPs and 1-yne-VCPs, the relative reactivities of 1-ene-VCP and 1-yne-VCP will be then discussed (section 2.1). Afterward, we

**Figure 3.** Potential energy surface of the [3+2] reaction of 1-ene-VCP.

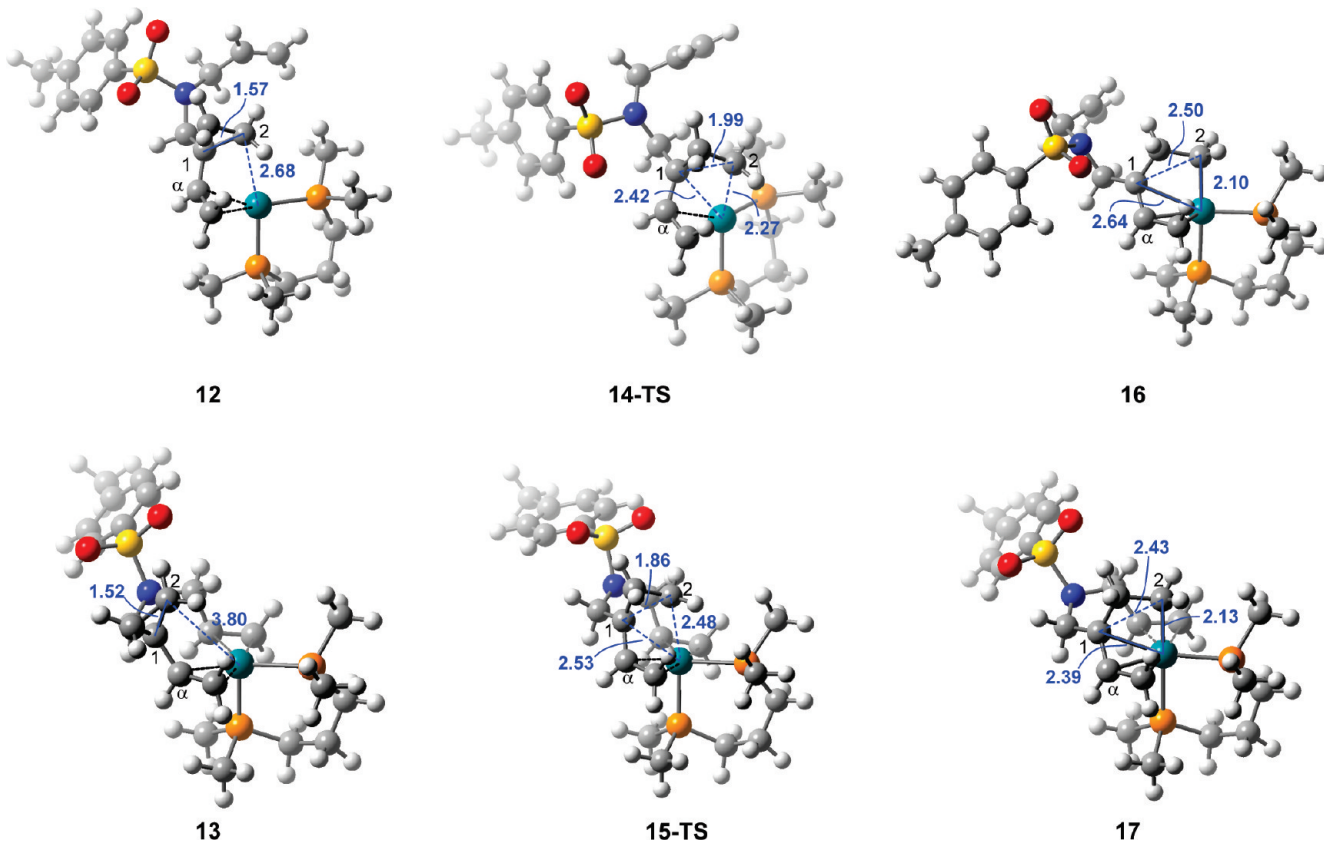
Scheme 4. Pathways for the Cyclopropane Cleavage Process (Energies in kcal/mol)

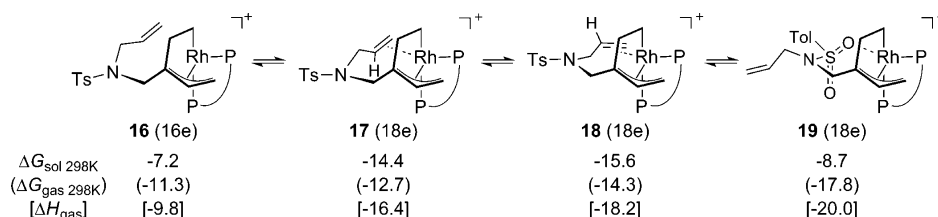
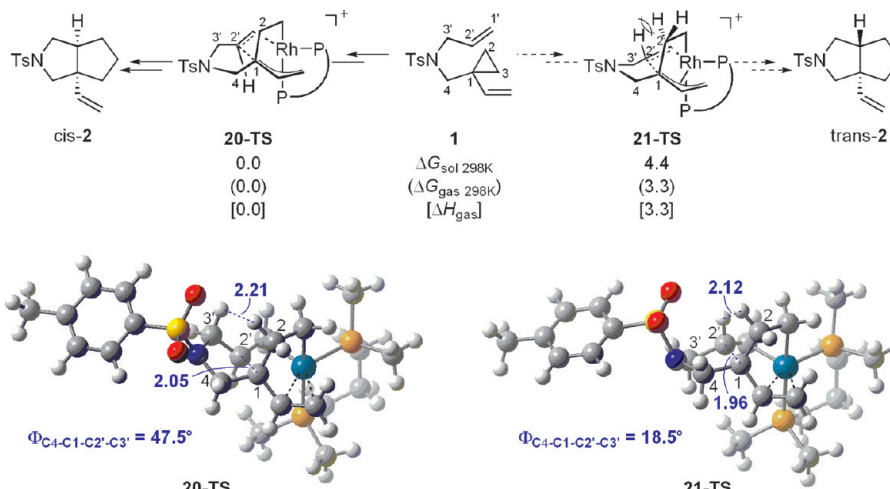
will focus on discussing the origins of the tether-controlled diastereoselectivity in the 1-yne-VCP participated [3+2] cycloaddition (section 2.2).

Part 1. DFT Investigation of the [3+2] Cycloaddition of 1-Ene-VCP. **1.1. Overview of the Catalytic Cycle.** We calculated the [3+2] cycloaddition mechanism of 1-ene-VCP **1** according to the proposed catalytic cycle shown in Figure 2. The whole potential energy surface is given in Figure 3. The key steps are ligand exchange, cyclopropane ring-opening, alkene insertion, and reductive elimination. These individual steps are discussed below, one by one.

1.1.1. The Ligand Exchange Step (Scheme 4 and Figure 4). The [3+2] catalytic cycle starts with the ligand exchange

between the product–Rh(I) complex **24**, which is generated in the previous catalytic cycle, and the substrate, 1-ene-VCP **1**. This ligand exchange reaction is exergonic by 5.0 kcal/mol, giving a 16-electron Rh(I) complex **12**, in which the VCP moiety binds to the rhodium center by both the vinyl group and the cyclopropane unit. In this complex, cyclopropane serves as a ligand, as demonstrated by the computed distance of the C2–Rh bond of 2.68 Å. Another evidence to support the coordination of cyclopropane to Rh is the elongation of the C1–C2 bond in the cyclopropyl unit compared to the C1–C2 bond in the free substrate **1** (1.57 Å in **12** vs 1.51 Å in **1**). In the reaction system, complex **12** is expected to be in equilibrium with another complex, **13**, which is also a 16-e complex and has the ene

**Figure 4.** Structures of intermediates and transition states **12–17**. Distances of concern are indicated by blue lines and are reported in angstroms.

Scheme 5. Equilibrium of the Ring-Opened Intermediates (Energies in kcal/mol)**Scheme 6.** DFT Study of the Diastereoselectivity of the 5,5-Ring Formation^a

^a Energies are given in kcal/mol. Distances of concern are indicated by blue lines and are reported in angstroms.

unit as an additional olefinic ligand. In complex **13**, the cyclopropyl unit is a bystander and does not act as a ligand (the computed distance between C2 and Rh in **13** is 3.80 Å). Complex **13** is less stable than **12** by 3.7 kcal/mol. Thus, after the ligand exchange process, complex **12** is the major species in the reaction system, compared to complex **13**.

1.1.2. The Cyclopropane Ring-Opening Step (Scheme 4 and Figure 4). In connection with intermediates **12** and **13**, two cyclopropane cleavage transition states, **14-TS** (without the ene complexation) and **15-TS** (with the ene part coordinated to the Rh center), can be located. In transition structure **14-TS**, the computed C1–C2 bond length in the cyclopropane unit is lengthened from 1.57 Å (in **12**) to 1.99 Å (in **14-TS**), and the distance between C2 and Rh is 2.27 Å (Figure 4). On the other hand, in transition structure **15-TS**, the computed C1–C2 bond length in the cyclopropane unit is lengthened from 1.52 Å (in **13**) to 1.86 Å (in **15-TS**), and the distance between C2 and Rh is 2.48 Å (Figure 4). It is found that **14-TS** is favored over **15-TS** by 7.7 kcal/mol. Interestingly, although the cyclopropane cleavage step is an oxidative addition process (Rh^I is converted to Rh^{III}), an additional ene complexation to increase the electron density on the rhodium center has no positive effect. This may be understood by the fact that the oxidative addition (i.e., the cyclopropane ring-opening) is reluctant to occur on a coordination-saturated metal center. Therefore, the cyclopropane cleavage pathway follows the sequence **1** → **12** → **14-TS** → **16**. During these transformations, one C–C bond of the cyclopropyl group is cleaved to give a π-allyl moiety, which binds to the rhodium center. The generated complex **16** has a triangular bipyramidal configuration, with both the methylene group and one of the phosphorus atoms at the axial positions, while the π-allyl ligand and the other phosphorus atom settle at the equatorial positions.

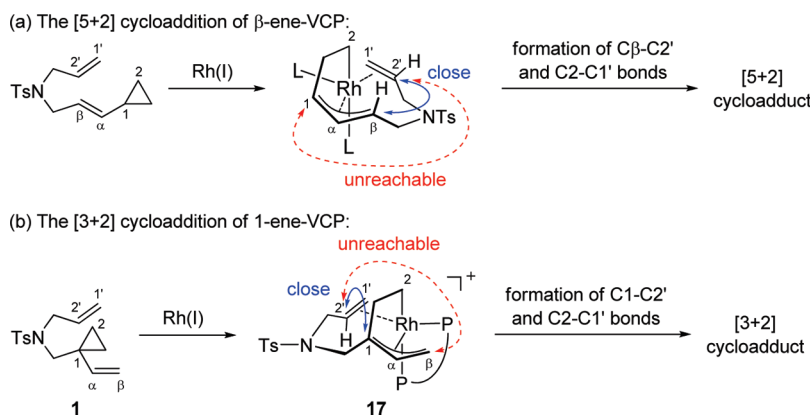
1.1.3. The Alkene Insertion Step (Schemes 5 and 6). Next, insertion of the olefin to the C(1)–Rh bond will take place to

give a six-membered rhodacycle, which settles the two stereogenic centers simultaneously. This process starts from alkene complexation, converting the 16-e complex **16** to the 18-e complex **17** (Scheme 5). In complex **17**, the alkene coordinates to the Rh center in a cis fashion, and this complex can undergo alkene insertion, leading to a cis-fused [3+2] cycloadduct. However, the alkene part in this complex can also coordinate to the Rh center in a trans fashion, leading to a more stable 18-e complex **18**. Intermediate **18** is more stable than **17** (by 1.2 kcal/mol) and **16** (by 8.4 kcal/mol) in terms of Gibbs free energy in solution. Since these complexes are interconvertable, the equilibrium will favor the formation of complex **18**. Therefore, cis insertion will follow the pathway **16** → **18** → **17** → **20-TS**, while trans insertion will follow the **16** → **18** → **21-TS** sequence. In the cis insertion transition state **20-TS**, the computed distance of the forming C1–C2' bond is 2.05 Å, and in the trans insertion transition state **21-TS**, the distance of the forming C1–C2' bond is 1.96 Å (Scheme 6). The cis insertion from **18** to **20-TS** requires 22.1 kcal/mol activation free energy, while direct trans insertion from **18** to **21-TS** requires 26.5 kcal/mol, which is 4.4 kcal/mol higher than the cis alkene insertion. Thus, the cis alkene insertion is favored, producing the 16-e complex intermediate **22**. The reasons behind this stereoselectivity will be discussed in section 1.2.

It is interesting to point out that there is also an 18-e complex **19** in equilibrium with complexes **16**, **17**, and **18** (Scheme 5). Complex **19** has a S=O···Rh interaction and is only slightly favored over intermediate **16** by 1.5 kcal/mol (the O–Rh bond distance is 2.35 Å). However, complex **19** is a minor species in the [3+2] reaction process because it is less stable than complex **18** by 6.9 kcal/mol in terms of free energy.

1.1.4. The Reductive Elimination Step. The final step of the [3+2] catalytic cycle is the reductive elimination reaction from intermediate **22** to give the product–catalyst complex **24**. This

Scheme 7



step requires an activation free energy of 16.4 kcal/mol. In the reductive elimination transition state **23-TS**, the computed distance of the forming C1'-C2 bond is 2.13 Å, and the C1'-Rh and C2-Rh distances are 2.29 and 2.27 Å, respectively (Figure 5). The alkene still coordinates to the Rh center in this transition state, as evidenced by the distances of the alkene to the Rh atom of 2.44 Å (C α -Rh) and 2.38 Å (C β -Rh).

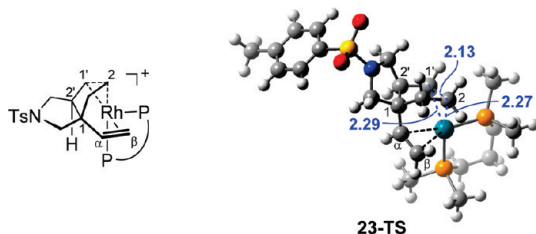


Figure 5. Reductive elimination transition structure **23-TS**. Distances of concern are indicated by blue lines and are reported in angstroms.

1.1.5. Overview of the Potential Energy Surface and Rationale of the [3+2]/[5+2] Cycloaddition Selectivity. The whole potential energy surface of the [3+2] catalytic cycle shown in Figure 3 indicates that the conversion from **1** to **18** via ligand exchange, cyclopropane cleavage, and olefin coordination is exergonic by 15.6 kcal/mol. The alkene insertion step (via **20-TS**) is the rate- and stereochemistry-determining step of the reaction and is irreversible. The cyclopropane cleavage (via **14-TS**) and reductive elimination steps (via **23-TS**) are facile. The overall activation energy barrier of the reaction is 22.1 kcal/mol (from **18** to **20-TS**) in terms of Gibbs free energy in solution. This activation free energy is in agreement with the fact that this [3+2] cycloaddition easily occurs at 80 °C.

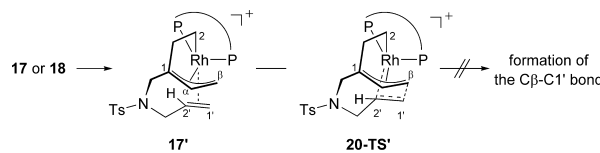
Having obtained the potential energy surface as well as the structure of intermediates and transition structures, we can now understand the reason why, in the present [3+2] reaction of 1-ene-VCP, the VCP moiety acts perfectly as a three-carbon component, rather than as a five-carbon component as in the [5+2] and [5+2+1] reactions of β -ene-VCPs. Previous DFT studies indicated that the [5+2] cycloaddition of β -ene-VCP is a stepwise reaction, in which the C-C bond between C β and the proximal internal olefin sp² carbon (C2') forms first and the second C-C bond forms subsequently via reductive elimination (Scheme 7a).^{5b,8} Our computational results indicated that the [3+2] cycloaddition of 1-ene-VCP is also a stepwise process. In contrast, in the [3+2] reaction process, the C β atom is far away from the complexed olefin, while the C1 atom and the internal olefin sp² carbon (C2') are in close proximity (Scheme

7b). Thus, the intramolecular olefin moiety could only insert into the C1-Rh bond, and then reductive elimination will forge the C1'-C2 bond to finish a [3+2] cycloaddition. This makes the competitive [5+2] cycloaddition impossible.¹⁷ The above analysis indicates that it is the geometry of the 1-ene-VCP substrate that forces the VCP moiety to act as a three-carbon unit.

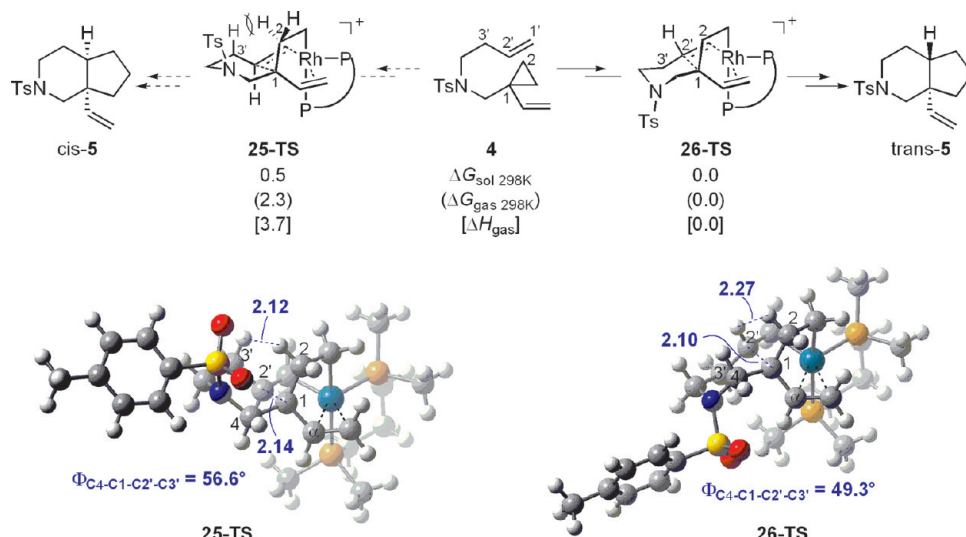
1.2. Understanding the Ring-Fusion Stereoselectivity in the 1-Ene-VCP [3+2] Cycloaddition. As shown in Scheme 2, in the [3+2] cycloaddition, 1-ene-VCP **1** afforded cis-fused 5,5-bicyclic compound **2** exclusively, whereas 1-ene-VCP **4** with a longer tether produced trans-fused 6,5-bicyclic compound **5**. We conducted calculations to understand how the tether length of the 1-ene-VCP substrate affects the ring-fusion stereoselectivity. The above-discussed potential energy surface has shown that alkene insertion is the stereochemistry-determining step in the [3+2] cycloaddition. Thus, by comparing and analyzing the diastereomeric alkene-insertion transition states in the formations of 5,5- and 6,5-bicyclic cycloadducts, we can figure out the key factors affecting the ring-fusion stereoselectivity.

1.2.1. Five-Membered Ring Formation. In the [3+2] cycloaddition of **1** to **2**, two diastereomeric alkene-insertion transition states, **20-TS** and **21-TS**, were located. It was found that cis insertion via **20-TS** is favored over trans insertion via **21-TS** by 4.4 kcal/mol (Scheme 6). Since the energy difference between the two diastereomeric transition states determines the ring-fusion selectivity, the computational result is consistent with the experimental observation that only cis-fused product **2** is obtained. Comparison of the two alkene-insertion transition

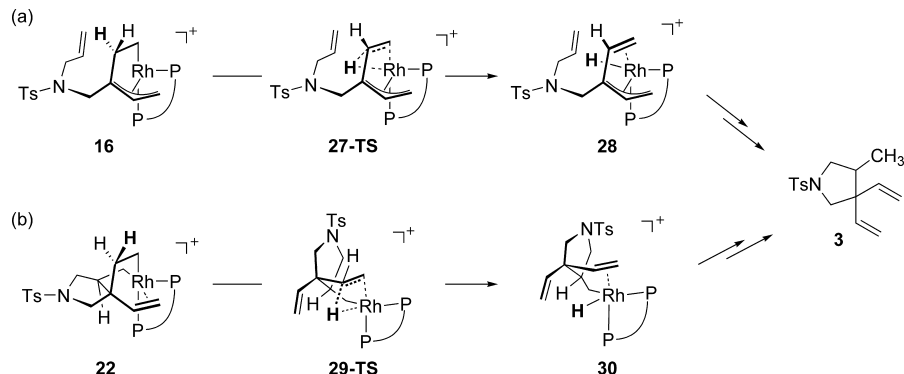
(17) One reviewer suggested that the ene moiety may complex to the trans position of C2 and then undergo insertion into the C α -Rh bond to give a [5+2] cycloaddition product (see scheme below). However, calculation suggested that this pathway requires a very high activation energy: $\Delta G(20-TS')_{\text{sol},298K}$ is 30.0 kcal/mol higher than $\Delta G(20-TS)_{\text{sol},298K}$. This indicates that, if the ene moiety was trans to the C2 atom, the alkene insertion could not occur. See Supporting Information for computational details of this possible pathway.



structure	18	17	20-TS	17'	20-TS'
$\Delta G_{\text{sol},298K}$ (kcal/mol)	0.0	1.2	22.1	5.0	52.1

Scheme 8. DFT Study of the Diastereoselectivity of the 6,5-Ring Formation^a

^a Energies are given in kcal/mol. Distances of concern are indicated by blue lines and are reported in angstroms.

Scheme 9. Two Possible Pathways for the β -Hydride Elimination

states reveals that torsional strain in the insertion transition states¹⁸ is responsible for the experimentally observed diastereoselectivity. In **20-TS**, the forming five-membered ring adopts a half-chair conformation, and the transition structure has a staggered conformation along the C1–C2' axis ($\Phi_{\text{C}4-\text{C}1-\text{C}2'-\text{C}3'} = 47.5^\circ$). However, in the energetically disfavored **21-TS**, the forming five-membered ring adopts an envelope conformation, and the transition structure has an eclipsed conformation along the C1–C2' axis ($\Phi_{\text{C}4-\text{C}1-\text{C}2'-\text{C}3'} = 18.5^\circ$), suggesting that **21-TS** suffers more severe torsional strain than **20-TS** does.

1.2.2. Six-Membered Ring Formation. In the [3+2] cycloaddition of **4** to **5**, two diastereomeric alkene-insertion transition states, **25-TS** and **26-TS**, were located. In contrast to the formation of the 5,5-bicyclic system, the formation of the 6,5-bicyclic system prefers to occur in a trans fashion. The trans insertion transition state **26-TS** is favored over the cis insertion transition state **25-TS** by 0.5 kcal/mol in solution (2.3 kcal/mol in the gas phase), which is in agreement with the experimental observation (Scheme 8). In both transition structures, the forming six-membered ring adopts a chair conformation but stretches to different directions. Both transition structures adopt staggered conformations along the C1–C2' axis ($\Phi_{\text{C}4-\text{C}1-\text{C}2'-\text{C}3'} = 56.6^\circ$ in **25-TS** and 49.3° in **26-TS**). This indicates that, different from the case of five-membered ring formation, the major factor that influences the relative stability of **25-TS** and **26-TS** is not torsional strain but 1,3-diaxial interaction. In **25-TS**, the C2 atom

is at the axial position and experiences steric repulsion with the axial C–H on the C3 atom (distance between H_{C2} and H_{C3'} is 2.12 Å). On the other hand, in **26-TS**, the C2 atom is at the equatorial position, and consequently no 1,3-diaxial interaction exists. In this transition structure, the distance between H_{C2} and the nearest H_{C2'} is 2.27 Å, leading to less steric repulsion than that in **25-TS**. Thus, the trans six-membered-ring formation transition state is more stable, favoring the formation of a trans-fused 6,5-bicyclic cycloadduct.

1.3. The β -Hydride Elimination Pathway. In the catalyst screening process, compound **3** was usually observed as the byproduct accompanying the desired [3+2] cycloadduct **2** (Table 1). It was assumed that compound **3** arose from a β -hydride elimination pathway, departing from the normal [3+2] reaction pathway. However, how this process occurred was unclear, and no mechanistic study of the β -hydride elimination on related reaction systems was reported. Therefore, we planned to disclose the detailed mechanism of this side reaction to obtain more mechanistic insights.

1.3.1. The β -Hydride Elimination Mechanism in $\text{Rh}(\text{dmppf})^+$ -Catalyzed [3+2] Cycloaddition. Through analyzing the catalytic cycle shown in Figure 3, we hypothesized that two intermediates in the [3+2] reaction process could possibly undergo the β -hydride eliminations to give byproduct **3** (Scheme 9). One possible intermediate for this process is complex **16**. This complex could undergo β -hydride elimination via **27-TS** to

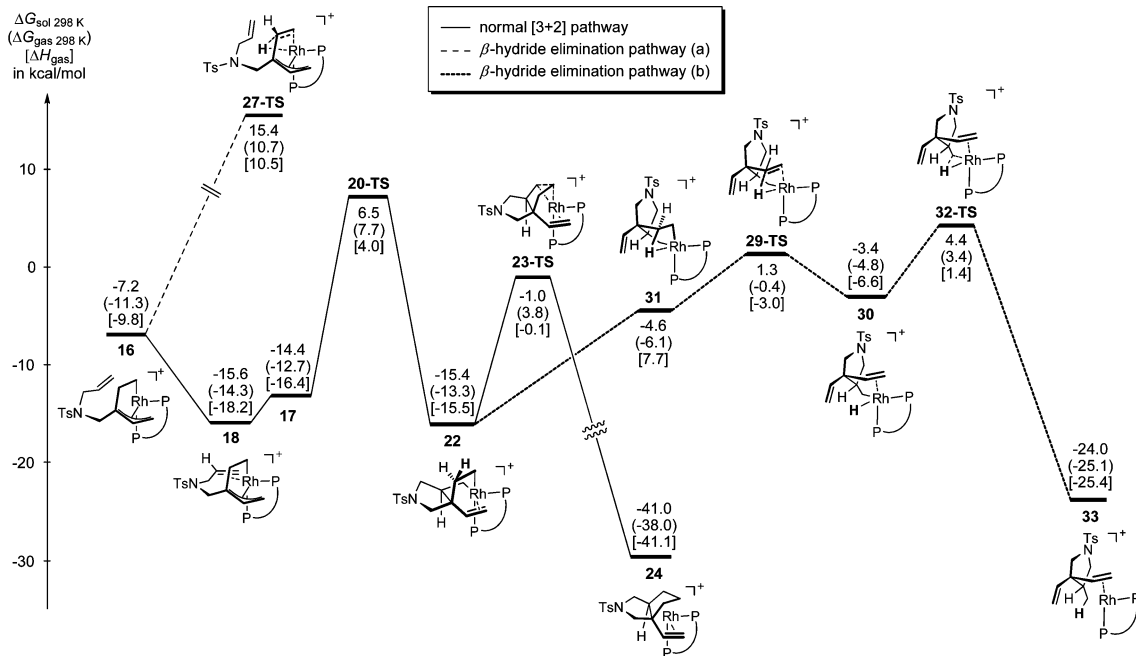


Figure 6. DFT-computed energy surfaces of the two β -hydride elimination pathways and a [3+2] pathway catalyzed by the cationic Rh–bidentate phosphine ligand complex.

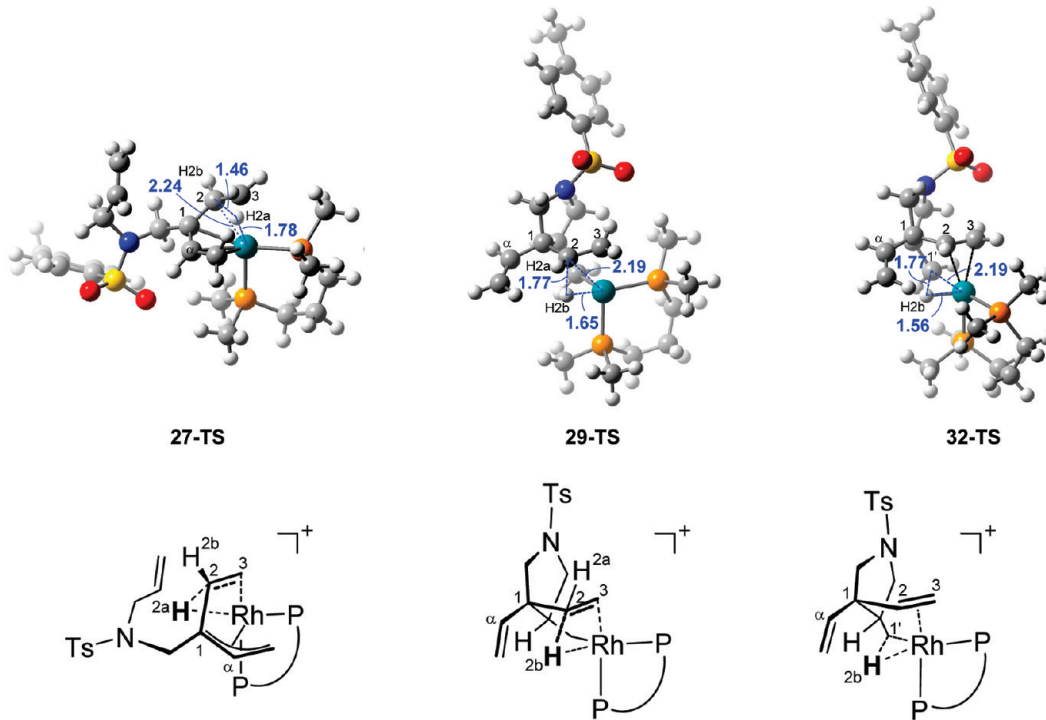


Figure 7. Key transition structures in the β -hydride elimination pathways. Distances of concern are indicated by blue lines and are reported in angstroms.

generate an 18-e η^5 -pentadienide–Rh(III) complex **28**, which could then be transformed to the final byproduct **3** via alkene insertion and reductive elimination. The other possible intermediate responsible for the generation of byproduct **3** is complex **22**. This complex could undergo β -hydride elimination via transition state **29-TS** to give complex **30**, which can then undergo reductive elimination to give compound **3**. We computed both pathways to examine which pathway is energetically favored. The DFT-computed potential energy surfaces for both β -hydride elimination pathways are given in Figure 6.

Computational results in Figure 6 indicate that the early-stage β -hydride elimination via **27-TS** from π -allyl rhodium intermediate **16** is energetically disfavored. This step requires an activation free energy as high as 31.0 kcal/mol (from the most stable intermediate **18**, Figure 6), which makes this pathway dramatically less favored than other competitive pathways. In the transition structure **27-TS**, the C2–H2a bond is lengthened from 1.09 Å (in **16**) to 1.46 Å, and the distance between Rh and H2a is 1.78 Å (Figure 7). The unfavorable steric distortion in the formation of a periplanar η^5 -pentadienide ligand from a

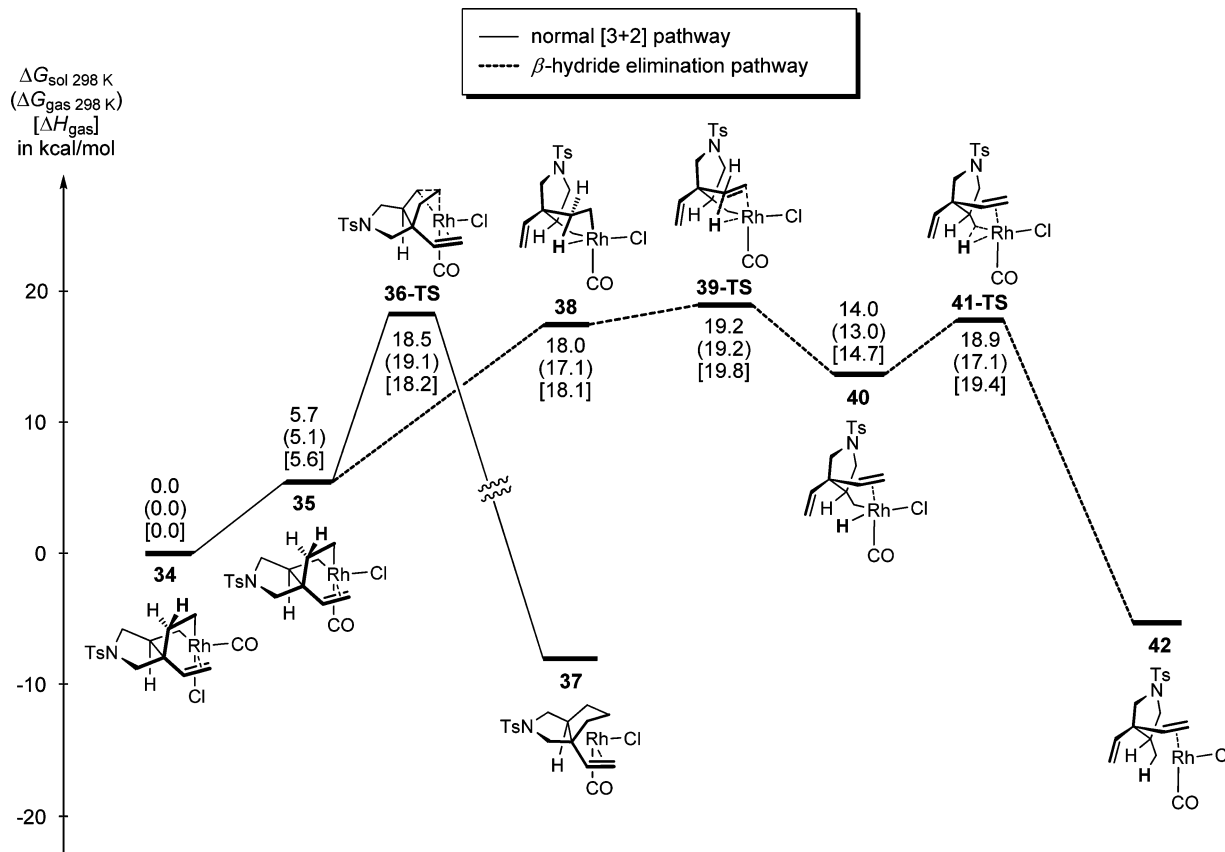


Figure 8. Potential energy surfaces for the normal [3+2] and β -hydride elimination pathways with $[\text{Rh}(\text{CO})_2\text{Cl}]_2$ as the catalyst.

cage-shaped ethylene- π -allyl ligand (in intermediate **16**) is probably the reason for such a high barrier. Therefore, this β -hydride elimination could be ruled out, and we then turned to consider another possible β -hydride elimination pathway from intermediate **22**. Although intermediate **22** is a 16-e complex with one empty binding site to facilitate β -hydride elimination, its cage-shaped structure with the ligands strongly coordinated to the rhodium center seems to prevent the approach of hydrogen on C2 migrating to rhodium for β -hydride elimination. Computational results indicated that a dramatic conformational change has to take place before β -hydride elimination takes places: first, the vinyl ligand dissociates to give one free binding site on rhodium, then an agostic C–H \cdots Rh interaction forms between hydrogen atom H2b and Rh (C2–H2b bond length, 1.16 Å; H2b \cdots Rh bond distance, 2.06 Å; intermediate **31** in Figure 6). After that, β -hydride elimination occurs to give 16-e intermediate **30** via **29-TS**, in which the C2–H2b and Rh–H2b distances are 1.77 and 1.65 Å, respectively. Intermediate **30**

then undergoes the final reductive elimination via **32-TS** to form the C1’–H2b bond, producing **33**, a complex between Rh and the β -hydride elimination product. In transition structure **32-TS**, the Rh–H2b and C1’–H2b distances are 1.56 and 1.77 Å, respectively. This pathway requires an activation free energy of 19.8 kcal/mol (from intermediate **22** to **32-TS**). The reductive elimination (via **32-TS**) is the most energy-demanding step in this pathway (Figure 6). Compared to the normal reductive elimination pathway (via **23-TS**), the calculated β -hydride elimination pathway is disfavored by 5.4 kcal/mol, indicating that the generation of byproduct **3** can be inhibited in the case of using $\text{Rh}(\text{dmpp})^+$ as the catalyst. This is in accordance with the catalyst screening results, showing that $\text{Rh}(\text{dppp})^+$ is the best catalyst to inhibit β -hydride elimination (Table 1).

1.3.2. The β -Hydride Elimination Mechanism in $[\text{Rh}(\text{CO})_2\text{Cl}]_2$ -Catalyzed [3+2] Cycloaddition. When $[\text{Rh}(\text{CO})_2\text{Cl}]_2$ instead of $[\text{Rh}(\text{dppp})]\text{SbF}_6$ is used as the catalyst for the [3+2] cycloaddition of **1**, the amount of β -hydride elimination product **3** increases significantly (see Table 1). To understand this, several key steps involved in the β -hydride elimination and the normal [3+2] pathways of 1-ene-VCP **1** using $[\text{Rh}(\text{CO})_2\text{Cl}]_2$ as catalyst¹⁹ have been computed (Figure 8). DFT calculations suggest that generation of the [3+2] cycloadduct from intermediate **34** starts from a ligand exchange to give intermediate **35**, which then undergoes reductive elimination via **36-TS** to give the [3+2] cycloadduct–Rh complex **37**. Generation of the normal

(18) For torsional interactions in the transition state (torsional steering), see: (a) Brown, F. K.; Houk, K. N. *J. Am. Chem. Soc.* **1985**, *107*, 1971. (b) Houk, K. N.; Paddon-Row, M. N.; Rondan, N. G.; Wu, Y.-D.; Brown, F. K.; Spellmeyer, D. C.; Metz, J. T.; Li, Y.; Loncharich, R. J. *Science* **1986**, *231*, 1108. (c) Evanseck, J. D.; Houk, K. H. *J. Am. Chem. Soc.* **1990**, *112*, 9148. (d) Wu, Y.-D.; Houk, K. N.; Paddon-Row, M. N. *Angew. Chem., Int. Ed. Engl.* **1992**, *31*, 1019. (e) Wu, Y.-D.; Li, Y.; Na, J.; Houk, K. N. *J. Org. Chem.* **1993**, *58*, 4625. (f) Martinelli, M. J.; Peterson, B. C.; Khau, V. V.; Hutchinson, D. R.; Leanna, M. R.; Audia, J. E.; Drost, J. J.; Wu, Y.-D.; Houk, K. N. *J. Org. Chem.* **1994**, *59*, 2204. (g) Ando, K.; Green, N. S.; Li, Y.; Houk, K. N. *J. Am. Chem. Soc.* **1999**, *121*, 5334. (h) Behnam, S. M.; Behnam, S. E.; Ando, K.; Green, N. S.; Houk, K. N. *J. Org. Chem.* **2000**, *65*, 8970. (i) Cheong, P. H.-Y.; Yun, H.; Danishefsky, S. J.; Houk, K. N. *Org. Lett.* **2006**, *8*, 1513. (j) Iafe, R. G.; Houk, K. N. *Org. Lett.* **2006**, *8*, 3469.

(19) It was believed that the catalytic species of the $[\text{Rh}(\text{CO})_2\text{Cl}]_2$ -catalyzed reaction is $\text{Rh}(\text{CO})\text{Cl}$. For references, see: (a) Reference 8a. (b) Reference 3c. (c) Lee, S. I.; Fukumoto, Y.; Chatani, N. *Chem. Commun.* **2010**, *46*, 3345.

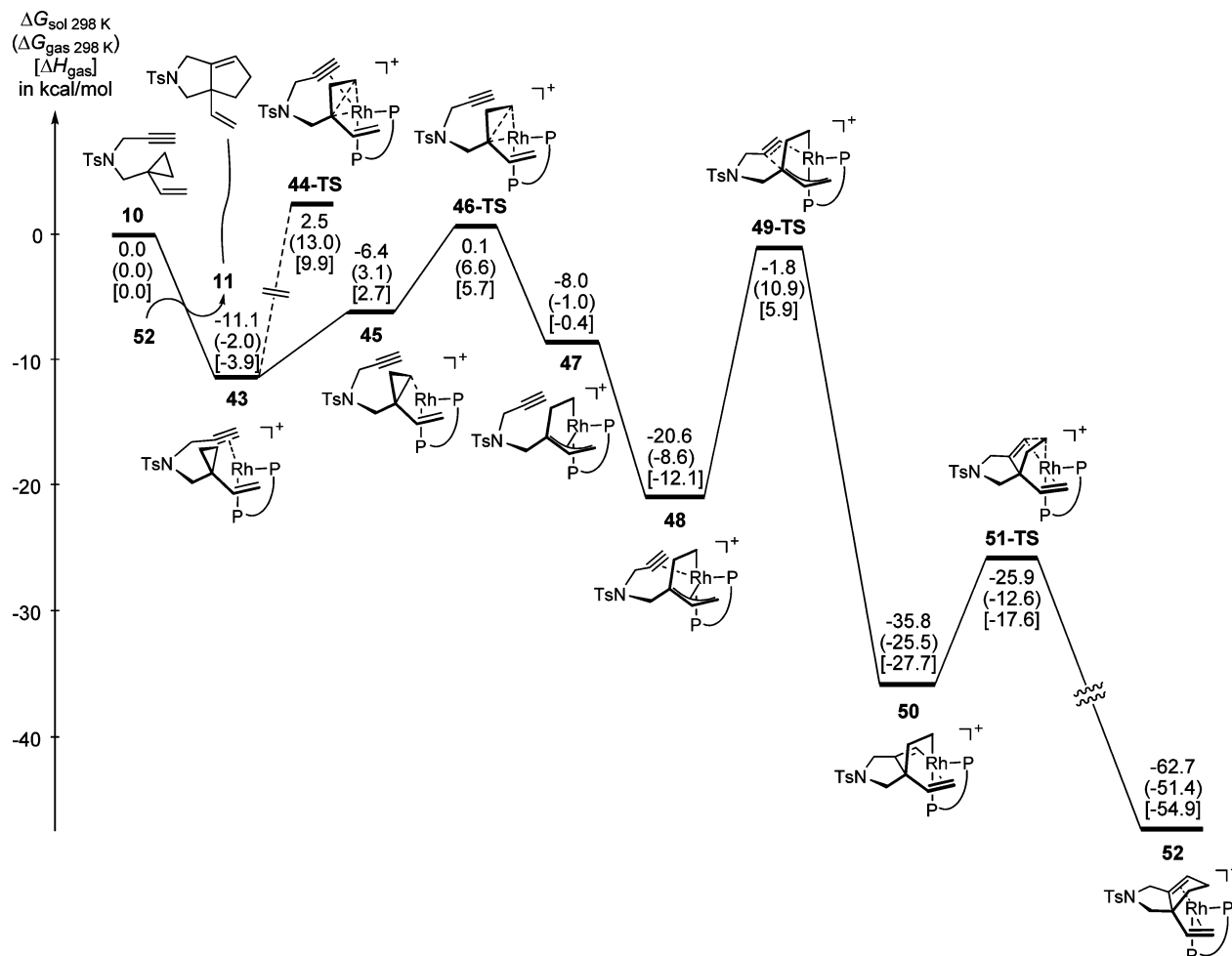


Figure 9. Potential energy surface of the [3+2] cycloaddition of 1-yne-VCP.

[3+2] cycloadduct–catalyst complex **37** from intermediate **34** requires an activation free energy of 18.5 kcal/mol.

In the competitive β -hydride elimination pathway, intermediate **35** first undergoes a conformational change to give an agostic intermediate **38**, which is then converted to a rhodium hydride intermediate **40** via β -hydride elimination transition state **39-TS**. From **34** to **39-TS**, the required activation free energy is 19.2 kcal/mol. The following reductive elimination to give the β -hydride elimination product–Rh complex **42** is easy, with an activation free energy of only 4.9 kcal/mol. Comparison of the [3+2] and β -hydride elimination pathways shows that the latter is slightly disfavored by 0.7 kcal/mol, indicating that the [3+2] cycloadduct **2** will be the major product, while the β -hydride elimination product **3** will also be present in a remarkable amount as the byproduct. This is in good agreement with the experimentally observed product distribution (2:3 = 4:1, see Table 1).

Why do $[\text{Rh}(\text{CO})_2\text{Cl}]_2$ and $[\text{Rh}(\text{dppp})]\text{SbF}_6$ have such different selectivities for the competitive [3+2] cycloaddition and β -hydride elimination pathways when they catalyze the [3+2] cycloaddition of 1-ene-VCP **1**? One major reason responsible for this difference is the fact that the use of bidentate phosphine ligand could decrease the activation energy barrier for the reductive elimination. For the reductive elimination in the normal [3+2] process, the $[\text{Rh}(\text{CO})_2\text{Cl}]_2$ -catalyzed reaction requires 18.5 kcal/mol (**34** to **36-TS**), while in the $[\text{Rh}(\text{dppp})]^+$ -catalyzed [3+2] reaction, only 14.4 kcal/mol (**22** to **23-TS**) is

required for this process. Meanwhile, the activation free energy barriers for both β -hydride elimination pathways are almost the same (for the $[\text{Rh}(\text{dppp})]\text{SbF}_6$ -catalyzed pathway, 19.8 kcal/mol is required from **22** to **32-TS**; for the $[\text{Rh}(\text{CO})_2\text{Cl}]_2$ -catalyzed pathway, 19.2 kcal/mol is required from **34** to **39-TS**). Therefore, in the $[\text{Rh}(\text{CO})_2\text{Cl}]_2$ -catalyzed reaction, the β -hydride elimination pathway becomes competitive with the normal reductive elimination pathway, leading to the generation of a remarkable amount of the β -hydride elimination byproduct. From a structural viewpoint, we believe that it is the steric bulkiness of the bidentate phosphine ligand that facilitates the reductive elimination step, thus inhibiting the β -hydride elimination pathway.²⁰

Part 2. DFT Study of the [3+2] Cycloaddition of 1-Yne-VCP. **2.1. Potential Energy Surface.** After detailed DFT investigation of the 1-ene-VCP participated [3+2] cycloaddition, we started to study the mechanism of the [3+2] cycloaddition of 1-yne-VCP substrate **10**. The reaction mechanisms of 1-ene-VCP and 1-yne-VCP participated [3+2] cycloadditions are similar. Therefore, in this part we will only briefly describe the catalytic cycle and the potential energy surface of the [3+2] reaction of 1-yne-VCP **10**.

2.1.1. Overview of the Potential Energy Surface. The DFT-computed potential energy surface of the [3+2] cycloaddition of 1-yne-VCP **10** is shown in Figure 9 (structures of the key

(20) Mondal, J. U.; Blake, D. M. *Coord. Chem. Rev.* **1982**, *47*, 205.

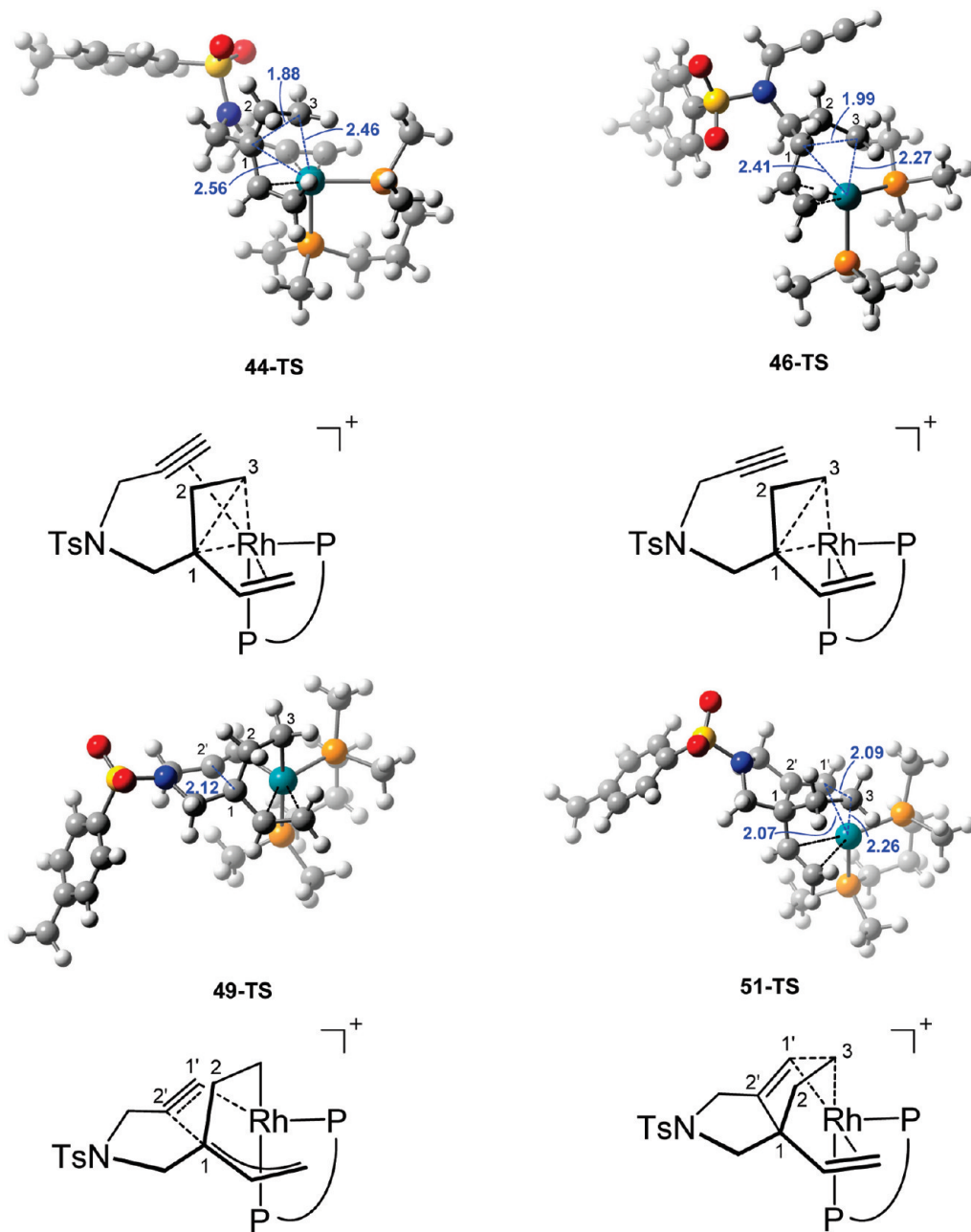
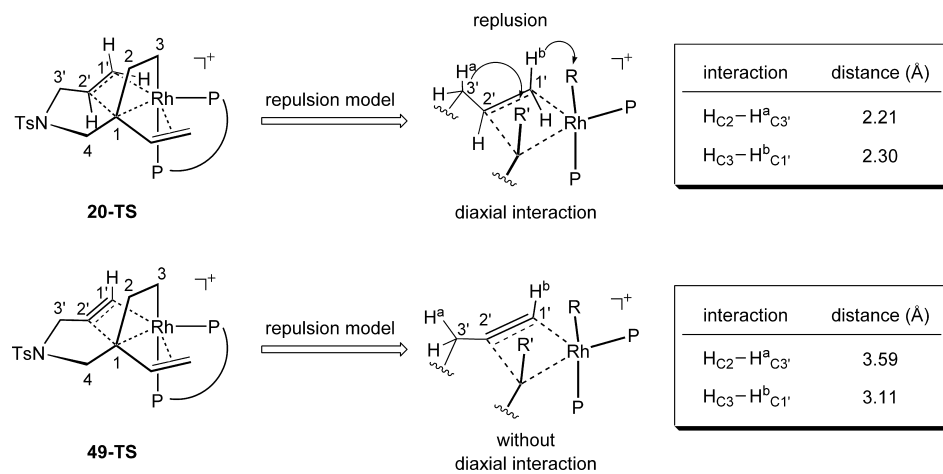


Figure 10. Key transition structures in the Rh(I)-catalyzed [3+2] cycloaddition reaction of 1-yne-VCP **10**. Distances of concern are indicated by blue lines and are reported in angstroms.

transition states involved are shown in Figure 10). Exergonic ligand exchange between substrate **10** and product–catalyst complex **52** releases the [3+2] cycloadduct **11** and regenerates substrate–catalyst complex **43** for the next catalytic cycle. This complex has a 16-e configuration, with both the vinyl group and the alkyne moiety complexed to the rhodium center. Cyclopropane cleavage of this yne-complexed intermediate can form a 18-e π -allyl rhodium complex **48** via **44-TS**, in which the distances between C1 and C3, C1 and Rh, and C3 and Rh are 1.88, 2.56, and 2.46 Å, respectively (Figure 10). However, similar to the [3+2] reaction of 1-ene-VCP, cyclopropane cleavage of this yne-complexed intermediate via **44-TS** is much more difficult. Thus, before cyclopropane cleavage, the yne moiety has to dissociate first from the Rh center, giving intermediate **45**. This intermediate is a 16-e complex, in which

the cyclopropane unit acts as a ligand (the distance between C2 and Rh is 2.68 Å). Intermediate **45** then undergoes the cyclopropane ring cleavage via **46-TS**, affording a 16-e complex **47**. In **46-TS**, the distances between C1 and C3, C1 and Rh, and C3 and Rh are 1.99, 2.41, and 2.27 Å, respectively (Figure 10). The followed step is the alkyne complexation to the Rh center, transforming the 16-e complex **47** to a more stable 18-e complex **48**. Subsequent alkyne insertion into the Rh–C bond via **49-TS** converts complex **48** into complex **50**, and this step requires an activation free energy of 18.8 kcal/mol. The final step of the [3+2] catalytic cycle is a very facile reductive elimination reaction, converting intermediate **50** to the product–catalyst complex **52** via transition state **51-TS**.

The computational results indicate that the most energy-demanding step in the [3+2] catalytic cycle of 1-yne-VCP

Scheme 10. Repulsion Models of the Alkene- and Alkyne-Insertion Transition States

is the alkyne-insertion reaction via **49-TS**. Similar to the [3+2] cycloaddition of 1-ene-VCP, the insertion step of the [3+2] reaction of 1-yne-VCP is both rate- and stereochemistry-determining. This [3+2] reaction requires an activation free energy of 18.8 kcal/mol, which is 3.3 kcal/mol lower than that required for the [3+2] reaction of 1-ene-VCP **1** (22.1 kcal/mol). This explains why 1-yne-VCP is generally more reactive than 1-ene-VCP in the Rh-catalyzed [3+2] cycloadditions.

2.1.2. Comparison of the [3+2] Cycloadditions of 1-Ene-VCP and 1-Yne-VCP: The Insertion and Reductive Elimination Steps. Our DFT calculations indicate that alkene insertion to the Rh–C bond is more difficult than alkyne insertion. It is known that alkene's HOMO is usually higher than that of alkyne,²¹ suggesting that alkene should be more reactive than alkyne to insert into the Rh–C bond if we consider the orbital interactions of alkene/alkyne's HOMO to the σ^* of the Rh–C bond. This is in contrast to the calculation results shown above. We propose that the higher insertion activity of alkyne than alkene into the Rh–C bond is due to steric reasons (Scheme 10). In the alkene-insertion transition state **20-TS**, the substituents on the alkene moiety experience several diaxial repulsions from the rhodacycles, while in the alkyne-insertion transition state **49-TS**, the substituents on the alkyne moiety stay far away from the rhodacycle, and no diaxial repulsion exists. Consequently, alkyne insertion is favored.

In the reductive elimination step, the reductive elimination from $\text{C}(\text{sp}^2)-\text{Rh}-\text{C}(\text{sp}^3)$ in the [3+2] cycloaddition is very easy, requiring less than 10 kcal/mol of activation free energy (**50** to **51-TS**). Compared to the 14.4 kcal/mol activation free energy for the corresponding reductive elimination step in the 1-ene-VCP [3+2] reaction (**22** to **23-TS**), the present result indicates that a migratory reductive elimination from $\text{C}(\text{sp}^2)-\text{Rh}-\text{C}(\text{sp}^3)$ is much more facile than a reductive elimination from $\text{C}(\text{sp}^3)-\text{Rh}-\text{C}(\text{sp}^3)$. The migratory reductive elimination transition state can be appreciated from the DFT calculations. In **51-TS**, the Rh and the $\text{C}(\text{sp}^2)$ carbon are almost intact (2.02 Å in **50** and 2.07 Å in **51-TS**), while the Rh–C bond is breaking (2.13 Å in **50** and 2.26 Å in **51-TS**), assembling a migration of $\text{C}(\text{sp}^3)$ to $\text{C}(\text{sp}^2)$. In contrast, in the potential energy surface of 1-ene-VCP, from **22** to **23-TS**, both Rh–C(sp³) bonds are breaking (2.10 to 2.30 Å and 2.11 to 2.27 Å, respectively), and this requires additional

energy compared to the migratory reductive elimination, where only one bond is breaking in the transition state.^{8a,22} Therefore, in most cases, the migratory reductive elimination to form a $\text{C}(\text{sp}^2)-\text{C}(\text{sp}^3)$ bond is much easier than a traditional reductive elimination to form a $\text{C}(\text{sp}^3)-\text{C}(\text{sp}^3)$ bond.

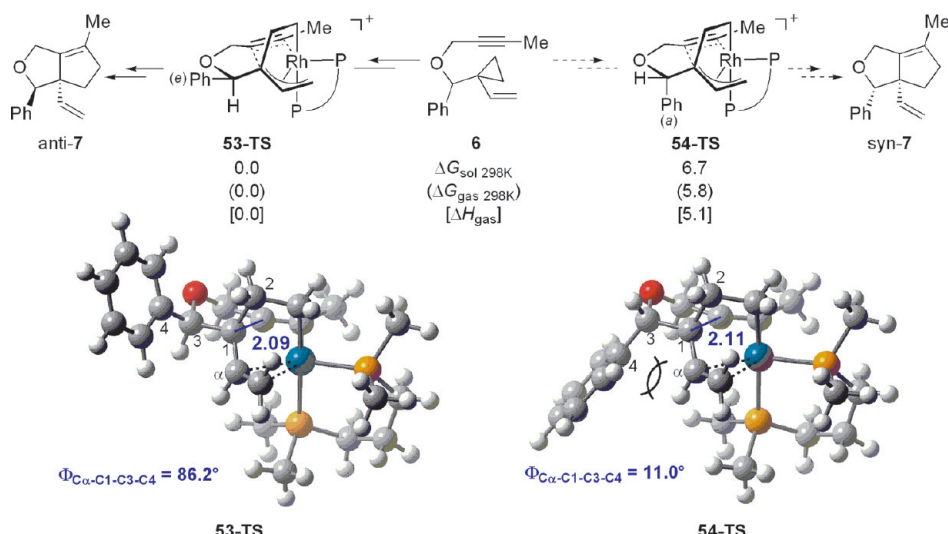
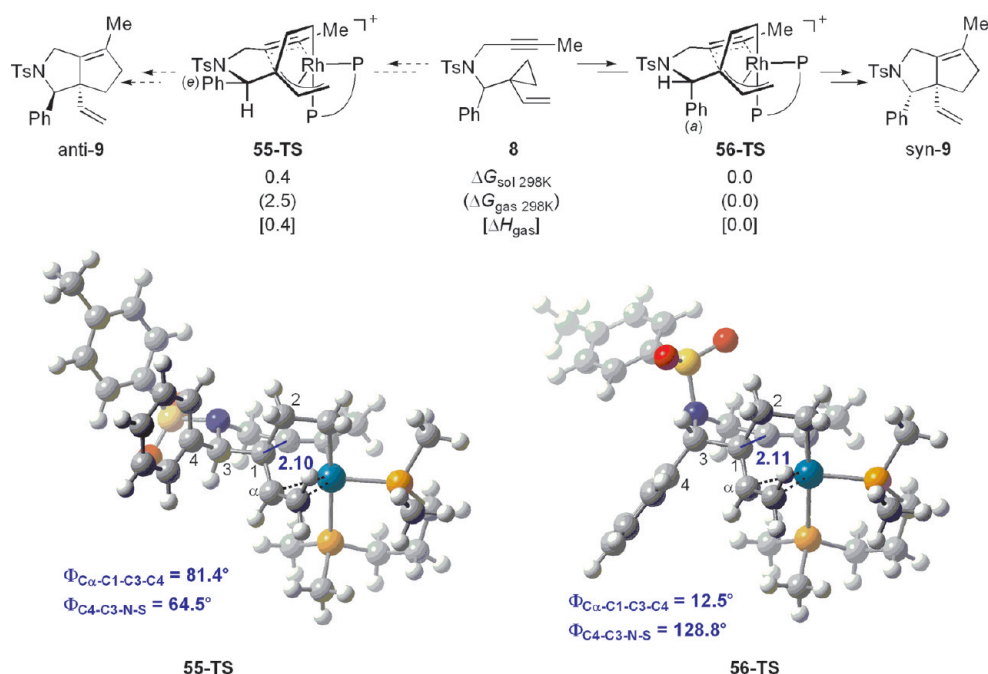
2.2. Understanding How the Tether Group of 1-Yne-VCPs Affects the Stereochemistry of the [3+2] Cycloaddition. It was observed that oxygen-tethered 1-yne-VCP **6** afforded cycloadduct **7** with anti stereochemistry, while tosylamide (TsN)-tethered 1-yne-VCP **8** produced cycloadduct **9** with syn stereochemistry (Scheme 2). Since the above discussion has established that the alkyne-insertion step controls the stereochemistry of the [3+2] cycloaddition, we could reveal the underlying factors affecting the stereochemistry by comparing and analyzing the diastereomeric alkyne-insertion transition states in the reactions of **6**→**7** and **8**→**9**.

2.2.1. The [3+2] Reaction of Oxygen-Tethered Substrate **6.** Two alkyne-insertion transition structures, **53-TS** and **54-TS**, were located for the [3+2] cycloaddition of 1-yne-VCP **6** (Scheme 11). Through further steps, transition states of **53-TS** and **54-TS** will lead to the final anti- and syn [3+2] cycloadducts, respectively. In **53-TS**, the phenyl group is at a pseudoequatorial position of the forming five-membered ring. The dihedral angle of $\Phi_{\text{Ca}-\text{C}1-\text{C}3-\text{C}4}$ is 86.2°, suggesting that less or no steric repulsion between the phenyl group and the C α of the π -allyl moiety exists. In contrast, in **54-TS**, the phenyl group is at a pseudoaxial position and has significant steric repulsion with the C α of the π -allyl moiety, as witnessed by a small dihedral angle of $\Phi_{\text{Ca}-\text{C}1-\text{C}3-\text{C}4}$ (11.0°). This steric penalty makes **54-TS** less stable than **53-TS** by 6.7 kcal/mol, indicating that generation of the anti **7** product is exclusive. This result is in very good agreement with the experimental observation.

2.2.2. The [3+2] Reaction of TsN-Tethered Substrate **8.** Two alkyne-insertion transition structures, **55-TS** and **56-TS**, were located for the [3+2] cycloaddition of 1-yne-VCP **8** (Scheme 12). Similar to the previous case, in **55-TS** (the anti alkyne-insertion transition state), the phenyl group sits at the pseudoequatorial position ($\Phi_{\text{Ca}-\text{C}1-\text{C}3-\text{C}4} = 81.4^\circ$), while in **56-TS** (the syn alkyne-insertion transition state), it occupies a pseudoaxial position ($\Phi_{\text{Ca}-\text{C}1-\text{C}3-\text{C}4} = 12.5^\circ$). Steric repulsion between the phenyl ring and the C α is still present in

(21) Jursic, B. S. *Tetrahedron* 1997, 53, 13285.

(22) Ozawa, F.; Mori, T. *Organometallics* 2003, 22, 3593, and references therein.

Scheme 11. O-Tether-Controlled Diastereoselectivity in the [3+2] Cycloaddition of 1-Yne-VCPs (Energies in kcal/mol)**Scheme 12.** NTs-Tether-Controlled Diastereoselectivity in the [3+2] Cycloaddition of 1-Yne-VCPs (Energies in kcal/mol)

the syn-insertion transition state **56-TS**, suggesting that the anti-insertion transition state **55-TS** would be favored if only this factor is taken into account. However, an additional steric interaction, the repulsion between the phenyl ring and the tosylamide tether, has also emerged in this case: in **55-TS**, the phenyl ring and the tosyl group are in a gauche relationship ($\Phi_{C4-C3-N-S} = 64.5^\circ$), introducing an additional remarkable steric repulsion. In **56-TS**, this negative factor is minimized since these two groups are in a trans relationship ($\Phi_{C4-C3-N-S} = 128.8^\circ$). We believe that this additional interaction between phenyl group and the tosyl group is more significant than the phenyl- $C\alpha$ steric repulsion, making **55-TS** less favorable than **56-TS**, and thus the syn [3+2] cycloadduct is preferred consequently. Our computational results show a 0.4 kcal/mol free energy difference in the cis and trans alkyne-insertion transition states, indicating that the formation of the syn product is favored with respect to the formation of the anti product. This calculated energy

difference is in agreement with the experimentally observed diastereoselectivity. From the above study, we can conclude that the steric repulsion between the tether and the substituent in the substrate in the alkyne-insertion transition states plays an important role in the stereoselectivity of the [3+2] reaction of 1-yne-VCPs.

Conclusion

The mechanisms of the Rh(I)-catalyzed intramolecular [3+2] cycloaddition reactions of 1-ene- and 1-yne-VCPs have been investigated by DFT calculations. This mechanistic study revealed the detailed processes of the catalytic cycles, the potential energy profiles, and the structures of intermediates and transition states, as well as the kinetic and thermodynamic parameters of these [3+2] cycloadditions. Rationalization of the experimental observations, including the ring-fusion stereoselectivity of 1-ene-VCPs, the tether-controlled stereochemistry

of the 1-yne-VCPs, and the β -hydride elimination side reaction of 1-ene-VCP, has also been achieved.

Insights obtained in the present DFT study include the following: (a) Mechanistically, we found that the [3+2] cycloadditions proceed through substrate–catalyst complex formation, cyclopropane cleavage, alkene/alkyne insertion, and reductive elimination steps. (b) Alkene/alkyne insertion is the rate- and stereochemistry-determining step of these multistep [3+2] processes. The $C\equiv C$ bond is more facile than the $C=C$ bond to undergo the insertion reactions into the Rh–C bonds, in accord with the experimental observation that the reactivity of 1-yne-VCPs is higher than 1-ene-VCPs in the [3+2] reactions. (c) DFT modeling shows that the ring conformations, 1,3-diaxial interactions, and tether/substituent repulsions in the alkene- and alkyne-insertion transition states synergistically affect the diastereoselectivities of the [3+2] cycloadditions. (d) The detailed mechanism of the generation of β -hydride elimination byproduct **3** is studied by DFT calculations, indicating that this pathway proceeds after the alkene-insertion step in the [3+2] catalytic cycle and consists of a sequence of transformations such as vinyl ligand dissociation, formation of the C–H agostic interaction, β -hydride elimination, and reductive elimination. DFT calculations revealed that the β -hydride elimination pathway can be inhibited dramatically when a bidentate phosphine ligand is used

in the reaction system, whereas this pathway is competitive with the [3+2] catalytic cycle if $[Rh(CO)_2Cl]_2$ is the applied catalyst without an additional ligand present. The present DFT study provides further understanding of the VCP chemistry, and we hope these insights serve as a mechanistic guide to inspire future discovery of new reactions and new chiral ligands.

Acknowledgment. We thank the Natural Science Foundation of China (20825205-National Science Fund for Distinguished Young Scholars, and 21072013), the Ministry of Education of China (108001), and the Ministry of Science and Technology (2011CB808603 and 2010CB833203-National Basic Research Programs of China 973 Programs) for financial support.

Note Added after ASAP Publication. There were errors in the version Published ASAP December 17, 2010, where there were no mention of the solvent (1,2-dichloroethane) used in the calculations, both in the text and the Supporting Information. The corrected version reposted on January 4, 2011.

Supporting Information Available: Computational details and Cartesian coordinates for all stationary points. This material is available free of charge via the Internet at <http://pubs.acs.org>.

JA107396T